IEEE Access
Multidisciplinary | Rapid Review | Open Access Journal

Received May 16, 2020, accepted June 2, 2020, date of publication June 12, 2020, date of current version June 25, 2020.

Digital Object Identifier 10.1109/ACCESS.2020.3001865

Linear Frequency Modulated Reverberation Suppression Using Non-Negative Matrix Factorization Methods, Dechirping Transformation and Modulo Operation

GEUNHWAN KIM, KYUNKYUNG LEE, (Member, IEEE), AND SEOKJIN LEE, (Member, IEEE)
School of Electronics Engineering, College of IT Engineering, Kyungpook National University, Daegu 41566, South Korea

Corresponding author: Seokjin Lee (sjlee6@knu.ac.kr)

This work was supported by the Agency for Defense Development (ADD) in Korea under Grant UD190005DD.

ABSTRACT In this study, we propose a reverberation suppression algorithm for linear frequency-modulated (LFM) pulse sonar systems using a non-negative matrix factorization (NMF) method. Because conventional NMF-based reverberation suppression algorithms are only applicable to continuous wave reverberation, we propose two pre-processing methods, namely dechirping transformation and modulo operation, to facilitate application of the NMF method to LFM reverberation. Moreover, we impose additional sparse constraints on the NMF method to improve its performance. To evaluate the proposed algorithm, an experiment involving simulated LFM reverberation is performed. The results thereof show improved detection performance at several signal-to-reverberation ratios and false alarm conditions. Moreover, the proposed algorithm is also applied to sea experiment data. According to the sea experiment analysis, the algorithm is able to suppress the LFM reverberation effectively and improve detection performance in practical LFM pulse sonar systems.

INDEX TERMS Active sonar, dechirping transformation, modulo operation, non-negative matrix factorization, reverberation suppression, sparse constraints.

I. INTRODUCTION

Active sonar is an underwater surveillance system that transmits pulses and analyzes received signals to detect, track, and classify underwater targets. During propagation through an underwater medium, the transmitted pulse is reflected by targets and scatterers to form the received signals; therefore, in addition to the target echoes, other unwanted reflections (termed reverberation) occur. Generally, an active sonar uses a matched filter to detect targets. The matched filter works to perform a sort of cross correlation between the transmitted pulse and the received signal. Because additive white Gaussian noise (AWGN) is not correlated by the transmitted pulse, the matched filter can work well in an AWGN environment. However, reverberation is highly correlated with the transmitted pulse; therefore, the reverberation interferes with the detection of the target echo by the matched filter. To improve the detection performance, extensive studies on reverberation suppression algorithms for active sonar have been conducted in the past decades [1]–[6].

We can categorize these studies on the basis of two approaches. The first approach involves designing a pulse waveform that is robust in a reverberation environment. Yves Doisy *et al.* classified the reverberation environment into three types, considering the beam steering angle and reverberation spectrum of each pulse [7]–[9]. From their study, we can conclude that the reverberation environment involves different reverberation interferences, depending on the transmitted pulse and the Doppler of the target to be detected. However, each type of pulse has its own merits; for example, some pulses provide an enhanced range or Doppler resolution, while others ensure transmission efficiency. Therefore, the theoretical reverberation performance cannot always be a priority, and some applications may demand enhancement of other characteristics [4], [10], [11].

To account for the merits of the different pulse types, the second approach can also be used. The most widely used and successful algorithm is that of the pre-whitening

The associate editor coordinating the review of this manuscript and approving it for publication was Yunlong Cai.

method that employs the auto-regressive (AR) model proposed by S. Kay [12]. However, this method assumes continuous wave (CW) reverberation, which has a narrowband spectrum. Thus, it is difficult to apply to linear frequency-modulated (LFM) reverberation, because it has a wideband spectrum. Although Camillet *et al.* attempted to use the AR pre-whitening method for LFM reverberation, their study did not provide a fundamental solution to the LFM reverberation problem [13]. To address this issue, Choi *et al.* proposed a pre-whitening method based on dechirping transformation [14]. Their method was different from that of Kay because it applied the dechirping transformation to produce the LFM reverberation as a tonal-like signal. Although Choi *et al.*'s method focuses on LFM reverberation suppression, it still presents some limitations. Choi *et al.*'s method assumes that strong reverberations from the sea surface or seabed are received, and they use these reverberations to design an inverse filter with an adjacent beam signal. Therefore, spreading reverberations that normally occurs cannot be suppressed. As an alternative, the principal component inversion (PCI) algorithm has been proposed [15]. This algorithm models the reverberation as the sum of several signals and finds a low-rank approximation of the signal matrix using singular value decomposition. As an improvement to the PCI algorithm, the signal subspace extraction (SSE) algorithm has been recently proposed [16]. The advantage of the SSE algorithm is that it models reverberation as a sum of the higher and lower reverberation parts. However, these methods are limited in that the reverberations and signal power must be estimated or properly selected. Further, they do not consider the characteristics of the pulse itself.

Recently, Lee *et al.* proposed a CW reverberation suppression algorithm based on non-negative matrix factorization (NMF) [17]. The NMF algorithm decomposes a non-negative matrix into two non-negative matrices with the advantage of representing the sparse features of the matrix [18]–[20]. In Lee *et al.*'s study, they used the NMF to obtain the segmented signal representation in the time-frequency domain. Because the NMF method is processed in the time-frequency domain, it has the advantage of reflecting the signal characteristics. They have thus successfully improved the detection performance by suppressing the CW reverberation. However, this algorithm was developed for CW pulse sonar systems and therefore fails when applied to LFM pulse sonar systems.

In this study, we propose an LFM reverberation suppression algorithm using the NMF method. Because conventional NMF methods cannot directly be applied in LFM reverberation environments, we introduce two pre-processing strategies, namely, the dechirping transformation and the modulo operation. We also propose the adoption of new sparse constraints based on the power of an estimated echo time basis to emphasize target echo signal components.

The remainder of this paper is organized as follows. In Section II, we present the problem statement, time-frequency model, and NMF model. The NMF algorithm with its CW applications is also discussed in this section. In Section III, we propose the novel LFM reverberation suppression algorithm using the NMF method with pre-processing and reconstruction of the target echo signal. In Sections IV and V, we present the simulation and sea experiment analysis, respectively, which are used to evaluate the proposed method. Finally, Section VI concludes this paper.

II. PRELIMINARIES

A. PROBLEM STATEMENT

In this study, we focused on reverberation suppression of LFM pulsed sonar systems, which are used in anti-submarine warfare. To detect silent submarines, modern sonar systems transmit various types of pulses at frequencies of several kilohertz or lower. CW and LFM pulses are primarily used; CW is superior for Doppler estimation, whereas LFM is superior for range estimation. A suitable pulse type is chosen depending on the situation. In addition, modern sonar systems generally use multiple sensors, such as a towed array sonar or a cylindrical array sonar, which perform the beamforming for discrimination of information from different angles. To develop a reverberation suppression algorithm, therefore, we need to understand the reverberation characteristics in these sonar systems. Doisy *et al.* [7]–[9] investigated these reverberation conditions in detail. In their study, they divided the reverberation region into three zones, namely, A, B, and C. Fig. 1 shows the differences between CW reverberation and LFM reverberation in terms of angle θ, steering angle θ_0, and ownership velocity v. The angle is expressed as $\sin\theta$. We can observe in Fig. 1 (a) that CW reverberation has a narrow-band spectrum, and it varies with the steering angle. Because the CW reverberation spectrum is narrow, zone A, formed by low Doppler targets, is small. Therefore, zone B is the area of primary concern. Zone C is not always included in the reverberation spectrum because the target is fast. Therefore, zone C is often disregarded. Because the LFM pulse has a wideband spectrum and a Doppler insensitive property, its reverberation is different from CW reverberation. Fig. 1 (b) shows that LFM reverberation has a wideband spectrum and is almost invariant regardless of the steering angle. Additionally, because the LFM pulse is Doppler insensitive, the spectrum of the target echo overwhelms this reverberation spectrum even in the presence of a moving target. Therefore, in LFM reverberation environments, zone B is suppressed, and zone A is dominant. In summary, the LFM reverberation suppression algorithm must have the ability to distinguish buried target echo signals from the wideband reverberation spectrum.

B. TIME-FREQUENCY MODEL OF RECEIVED SIGNAL

The transmitted pulse used in active sonar can be expressed as

$$s_p(t) = \cos\left(2\pi f_c t + \phi(t)\right), \quad 0 \le t \le T, \tag{1}$$

where f_c is the center frequency, $\phi(t)$ is the phase, and T is the length of the pulse. The phase of an LFM pulse can be

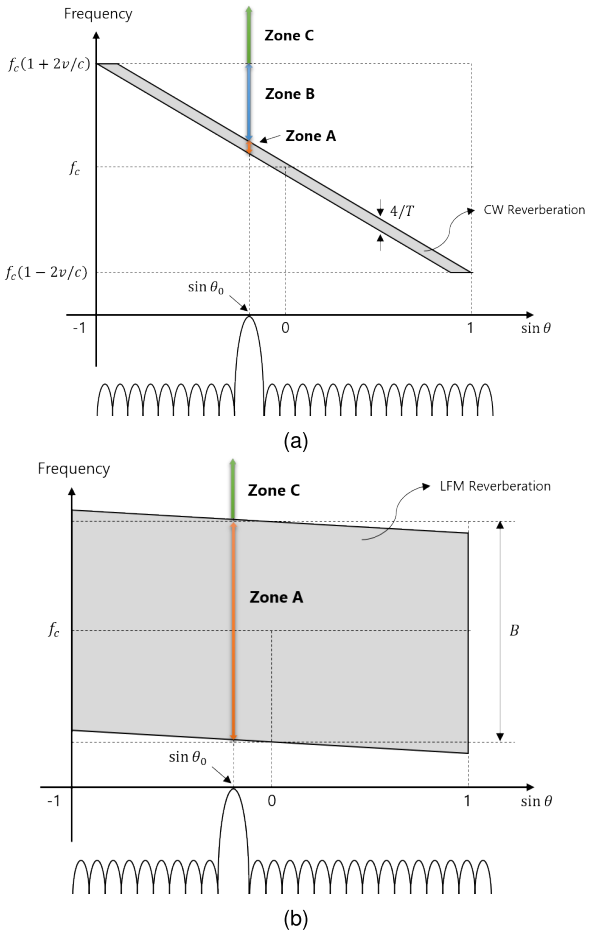

FIGURE 1. Comparison of reverberation environments: (a) CW pulse and (b) LFM pulse.

expressed as

$$\phi_{LFM}(t) = 2\pi \frac{1}{2}\gamma\, t^2, \quad 0 \le t \le T, \tag{2}$$

where $\gamma = B/T$ is the chirp rate of the LFM pulse, and B is the bandwidth of the LFM pulse.

The received beam signal can be expressed as

$$x(t) = s_e(t) + s_r(t) + n(t), \tag{3}$$

where $s_e(t)$ is the received target echo signal, $s_r(t)$ is the reverberation signal, and $n(t)$ is ambient noise, which is modeled as a zero-mean Gaussian distribution.

The target echo signal can be modeled as

$$s_e(t) = a_e s_p(\eta_e(t - \tau_e)), \tag{4}$$

where a_e, η_e, and τ_e are an attenuation factor, a Doppler scale factor, and the time delay of the target echo, respectively.

During the propagation in the underwater channel, the transmitted pulse is reflected by many scatterers. This causes time, frequency, and phase dispersion or spreading. Consequently, an unwanted signal, referred to as a reverberation, occurs as interference. Because reverberation signals are generally considered as nonstationary, some studies have

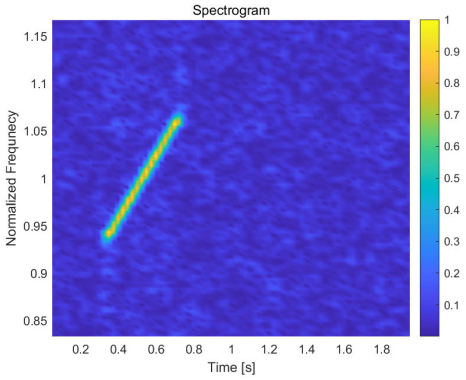

FIGURE 2. Spectrogram of target echo of LFM pulse.

been devoted to synthesizing the power spectral density of nonstationary reverberation using AR modeling [21], [22]. However, we assumed that the reverberation suppression algorithm is conducted with block units, and the condition of being locally stationary is satisfied in the processing block. Therefore, we used a straightforward point scattering reverberation model. Reverberation signals can be modeled as the sum of many reflected signals by scatterers and can be expressed as

$$s_r(t) = \sum_i a_i s_p(\eta_i(t - \tau_i)), \tag{5}$$

where a_i is an attenuation factor, η_i is a Doppler scale factor, and τ_i is the time delay of the ith scatterer. The number of scatterers depends on various factors, including the oceanic environment, beam width, and bandwidth, which cause the probability characteristics of the matched filter output to change. However, describing the detailed relationship between the number of scatterers and the various oceanic factors is beyond the scope of this paper [2].

To observe the information in the received signal, the time-frequency representation is often used. To convert the time signal to the time-frequency domain, a short time Fourier transform (STFT) is generally used as follows [23]:

$$X(k,n) = \sum_{m=-\infty}^{\infty} x(m)w(m - n\Delta h)e^{-j2\pi km/l_w}, \tag{6}$$

where $x(m)$ is the sampled beam signal, $w(m)$ is the window function of l_w samples, m is the index of each sample, and Δh is the hop size. Further, k and n are the frequency bin and time frame bin indexes, respectively. The magnitude square of (6) yields the spectrogram $\mathbf{V}$ as follows:

$$[\mathbf{V}]_{(k,n)} = |X(k,n)|^2, \tag{7}$$

where $[\mathbf{V}]_{(k,n)}$ is the (k,n) element of matrix $\mathbf{V}$.

Fig. 2 provides an example of a spectrogram of the LFM target echo arriving at 0.33 s in a noise-limited environment. To calculate a spectrogram, STFT is performed with a 0.1 s Hamming window and a 75% overlap (i.e., hop size of 25% of window length). Note that the amplitude is normalized to the maximum value and is the same thereafter, unless

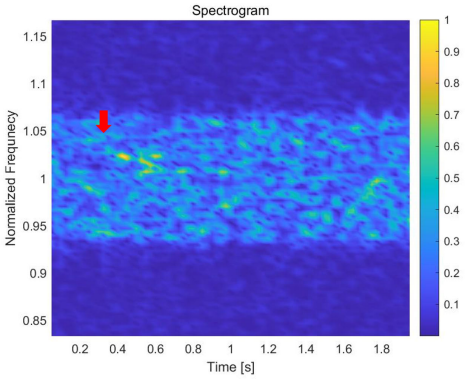

FIGURE 3. Spectrogram of target echo with reverberation noise.

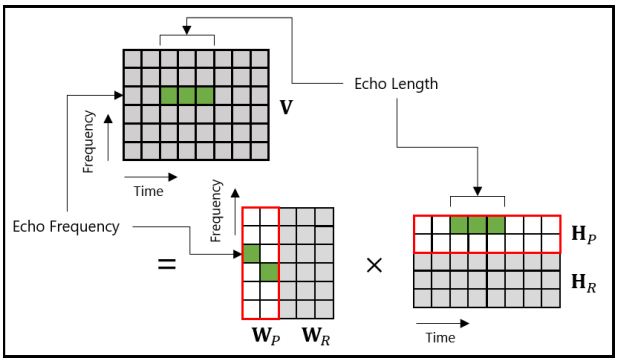

FIGURE 4. NMF scheme of two different parts, target echo ($\mathbf{W}_P$, $\mathbf{H}_P$) and reverberation ($\mathbf{W}_R$, $\mathbf{H}_R$).

otherwise stated. Fig. 3 presents the spectrogram of LFM reverberation with a buried target echo. Because the reverberation spectrum masks the target echo signal, it is difficult to recognize that the target is present in this spectrogram (indicated by the red arrow) [1], [2], [17].

C. CW REVERBERATION SUPPRESSION USING NON-NEGATIVE MATRIX FACTORIZATION

From the non-negative spectrogram in (7), we could develop the NMF algorithm. NMF decomposes the non-negative matrix into a multiplication of two non-negative matrices. The NMF model is expressed as

$$\mathbf{V} = \mathbf{WH} + \mathbf{E}, \tag{8}$$

where $\mathbf{V} \in \mathbb{R}^{+}_{K\times N}$, $\mathbf{W} \in \mathbb{R}^{+}_{K\times L}$, $\mathbf{H} \in \mathbb{R}^{+}_{L\times N}$, and $\mathbf{E} \in \mathbb{R}^{+}_{K\times N}$. As mentioned previously, the matrix $\mathbf{V}$ is the spectrogram of the input signals with K frequency bins and N time frames, and $\mathbf{W}$ and $\mathbf{H}$ are the frequency and time basis matrices, respectively. Further, L is the rank of the NMF. The matrices $\mathbf{W}$, and $\mathbf{H}$ can be estimated from the input spectrogram $\mathbf{V}$ by the multiplication update (MU) rule using a cost function with the Kullback–Leibler (KL) divergence [19]. Virtanen [20] proposed a generalized update rule that can be expressed as

$$\mathbf{W} \leftarrow \mathbf{W} \circ \frac{\nabla^{-}_{\mathbf{W}} C(\mathbf{W},\mathbf{H})}{\nabla^{+}_{\mathbf{W}} C(\mathbf{W},\mathbf{H})}, \tag{9}$$

$$\mathbf{H} \leftarrow \mathbf{H} \circ \frac{\nabla^{-}_{\mathbf{H}} C(\mathbf{W},\mathbf{H})}{\nabla^{+}_{\mathbf{H}} C(\mathbf{W},\mathbf{H})}, \tag{10}$$

where $\circ$ and the fractions represent the Hadamard multiplication (element-wise product) and element-wise divisions, respectively. $\nabla^{+}_{\mathbf{W}} C(\mathbf{W},\mathbf{H})$, $\nabla^{-}_{\mathbf{W}} C(\mathbf{W},\mathbf{H})$ and $\nabla^{+}_{\mathbf{H}} C(\mathbf{W},\mathbf{H})$, $\nabla^{-}_{\mathbf{H}} C(\mathbf{W},\mathbf{H})$ are the positive and negative parts of gradient $\nabla_{\mathbf{W}} C(\mathbf{W},\mathbf{H})$ and $\nabla_{\mathbf{H}} C(\mathbf{W},\mathbf{H})$, respectively. Because the positive and negative parts have non-negative values, the gradient can be expressed as

$$\nabla_{\mathbf{W}} C(\mathbf{W},\mathbf{H}) = \nabla^{+}_{\mathbf{W}} C(\mathbf{W},\mathbf{H}) - \nabla^{-}_{\mathbf{W}} C(\mathbf{W},\mathbf{H}), \tag{11}$$

$$\nabla_{\mathbf{H}} C(\mathbf{W},\mathbf{H}) = \nabla^{+}_{\mathbf{H}} C(\mathbf{W},\mathbf{H}) - \nabla^{-}_{\mathbf{H}} C(\mathbf{W},\mathbf{H}). \tag{12}$$

Recently Lee and Lim proposed a CW reverberation suppression algorithm using an NMF method [17]. To establish the frame of the algorithm, they first divided the input signal spectrogram into the target echo and reverberation parts, and then applied different constraints to each basis. Because of this division, NMF can estimate the information of the target echo and the reverberation separately. Fig. 4 shows their proposed NMF scheme. The frequency basis matrix $\mathbf{W}$ and the time basis matrix $\mathbf{H}$ are expressed as

$$\mathbf{W} = \begin{bmatrix} \mathbf{W}_P & \vdots & \mathbf{W}_R \end{bmatrix}, \tag{13}$$

$$\mathbf{H} = \begin{bmatrix} \mathbf{H}_P \\ \cdots \\ \mathbf{H}_R \end{bmatrix}, \tag{14}$$

where $\mathbf{W}_P \in \mathbb{R}^{+}_{K\times L_P}$ is the target echo part of the frequency basis matrix, $\mathbf{W}_R \in \mathbb{R}^{+}_{K\times L_R}$ is the reverberation part of the frequency basis matrix, $\mathbf{H}_P \in \mathbb{R}^{+}_{L_P\times N}$ is the target echo part of the time basis matrix, and $\mathbf{H}_R \in \mathbb{R}^{+}_{L_R\times N}$ is the reverberation part of the time basis matrix. Further, L_P and L_R are the basis numbers of the target echo and the reverberation, respectively, and $L = L_P + L_R$. Then, the NMF model (8) can be expressed as

$$\mathbf{V} = \mathbf{W}_P\mathbf{H}_P + \mathbf{W}_R\mathbf{H}_R + \mathbf{E}, \tag{15}$$

where $\mathbf{E} \in \mathbb{R}^{+}_{K\times N}$ is an error matrix. The additivity assumption of the target echo ($\mathbf{W}_P\mathbf{H}_P$) and reverberation ($\mathbf{W}_R\mathbf{H}_R$) in the NMF model (15) is reasonable because it is consistent with the signal model (3).

In Lee's method, the CW target echo components were shown as horizontal lines in the spectrogram. This indicates that CW target echo information is concentrated in a narrow or single frequency bin and is continuous along several time bins. Fig. 4 shows the meaning of this assumption. In the figure, matrix $\mathbf{V}$ is decomposed as $\mathbf{W}_P$, $\mathbf{W}_R$, $\mathbf{H}_P$, and $\mathbf{H}_R$. As $\mathbf{W}_P$ is fixed in advance, after decomposition, the information of the target (green cell) in $\mathbf{V}$ appears in a form in which a specific region of the $\mathbf{H}_P$ matrix is activated on a specific frequency basis of the $\mathbf{W}_P$ matrix. Therefore, we can

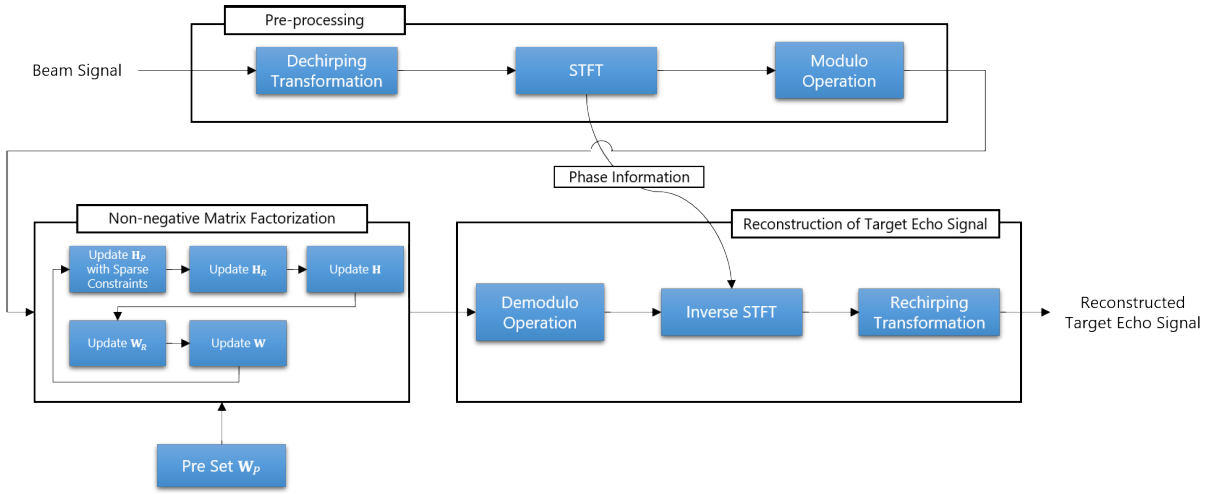

FIGURE 5. Block diagram of proposed LFM reverberation suppression scheme.

reconstruct the target echo signal from $\mathbf{W}_P$ and $\mathbf{H}_P$, which are indicated inside the red rectangles.

On the basis of the above explanation and Fig. 4, Lee's NMF algorithm is conducted as per the following process. $\mathbf{W}_P$ is initialized with a set of one-hot encoded vectors, which represent the specific Doppler target echoes and are fixed during the update. Other matrices are then updated using the MU rule with several constraints until convergence is achieved. Finally, echo information is reconstructed from the target echo basis matrices.

III. PROPOSED LFM REVERBERATION SUPPRESSION USING THE NMF METHOD

A. CONTRIBUTION OF THE PROPOSED METHOD

As we explained in Section II, LFM reverberation differs from CW reverberation, and the conventional NMF method cannot be applied to an LFM sonar system because, in this method, it is assumed that the CW target echo is shown as a continuous straight line in the spectrogram. However, the LFM signal is shown as an inclined diagonal line from which the frequency varies over time. Additionally, the LFM reverberation has a broader spectrum. Therefore, if we apply the conventional NMF method in LFM sonar systems, it is difficult to distinguish target echo information.

To overcome these problems, we modified Lee's NMF-based CW reverberation suppression algorithm to suit LFM reverberation. Fig. 5 shows the proposed LFM reverberation suppression scheme. When a beam signal is received, pre-processing steps are applied. After pre-processing, the beam signal is converted to a non-negative spectrogram suitable for use with the NMF algorithm. The modified NMF algorithm is then iteratively applied until it converges. Finally, the target echo signal is reconstructed by applying the inverse processing of the pre-processing steps in reverse order.

The main contributions of this study are the design of two pre-processing methods, namely the dechirping transformation and the modulo operation, and the update operation of the target echo time basis matrix $\mathbf{H}_P$ that employs a sparse constraint. The first pre-processing method, the dechirping transformation, is adopted to transform a diagonal LFM target echo into a straight line similar to the case with a CW target echo. The other pre-processing step, the modulo operation, is adopted to compensate for target echo information that is split by block processing. $\mathbf{H}_P$ update with sparse constraint is adopted to suppress more reverberation energy and emphasize the target echo signal.

B. PRE-PROCESSING

Typically, the signal is sampled and processed with block units. If we denote vector $\mathbf{x}$ as the entire received signal and divide it into Q block units, it can be expressed as follows:

$$\mathbf{x} = \left[\mathbf{x}_1^T \cdots \mathbf{x}_q^T \cdots \mathbf{x}_Q^T\right]^T, \tag{16}$$

where $\mathbf{x}_q$ is the qth block signal and can be expressed as follows:

$$\mathbf{x}_q = \left[x\left((q-1)M+1\right), \cdots, x\left((q-1)M+M\right)\right]^T. \tag{17}$$

where M is the number of samples corresponding to the processing block, which is set to the pulse length for convenience in processing.

The dechirping transformation method aims to change the LFM target echo into a horizontal line before it is applied to the NMF algorithm. When the LFM pulse is defined as (2), the dechirping vector can be defined as

$$\mathbf{g} = \exp\left(-j2\pi\frac{1}{2}\gamma\left(\frac{m}{f_s}\right)^2\right), \quad m = 0, \cdots, M-1, \tag{18}$$

where f_s is the sampling frequency, and γ is the chirp rate of the LFM pulse. Then, the dechirping transformation for the qth block signal can be performed as

$$\mathbf{x}_{Dec,q} = \mathbf{x}_q \circ \mathbf{g}. \tag{19}$$

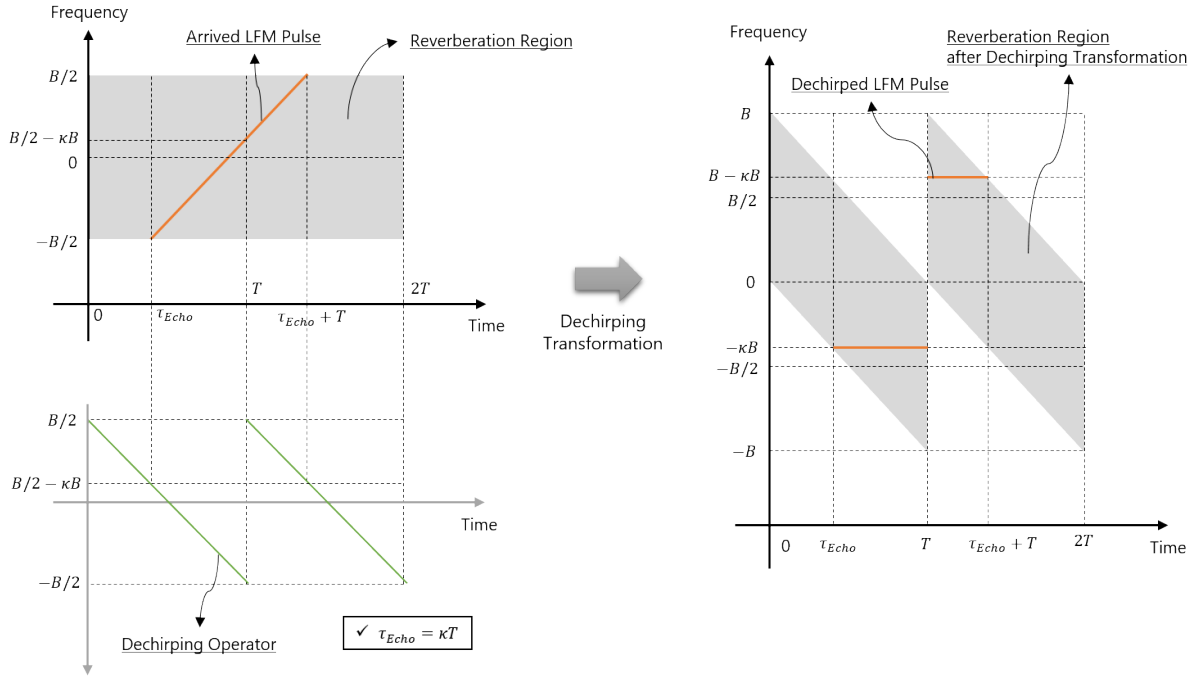

FIGURE 6. Dechirping transformation.

Note that the length of the processing block is equal to the length of the pulse and dechirping vector. In addition, we assume that the Doppler of the received target echo does not influence the dechirping transformation results because the LFM pulse is Doppler insensitive. Moreover, we assume that the target is expected to have a low Doppler. That is, it is not expected that a large difference will occur in the slant line of the LFM, and the echo information will be included in the same frequency bin after the transformation. We also assume that reverberation does not influence the dechirping transformation because the reverberation spreads, and the dechirping transformation is not completely performed. In contrast to reverberation, the target has a higher coherence, and its information will be delivered through the dechirping transformation. Even if the reverberation component is dechirped, the effect of reverberation is small. This is because only very few reverberation components with arrival times near the target echo in the time domain are located in the frequency bins near the target after transformation. Therefore, if a specific LFM pulse arrived at $\tau_{Echo} = \kappa T$ in the processing block, where κ is a constant between 0 and 1, we can expect that it will be located at $-\kappa B$ after the dechirping transformation. Furthermore, we can estimate the effect of the cut signal by block processing. Therefore, the received LFM signal, which includes the target echo and reverberation, will be shown as a parallelogram. Fig. 6 shows the dechirping transformation in detail.

It is common and unavoidable to process the input signal in block units, and there is a possibility that the received LFM pulse would be cut, as shown in Fig. 6. If we apply the NMF algorithm separately without other considerations, target echo information will disappear because NMF uses continuity information of the echo signal. If we increase the block length to prevent this phenomenon, the dechirping transformation spreads the LFM reverberation spectrum over the transformed frequency axis as in Fig. 7, which shows an example with a spectrum with double the length. In this case, the NMF algorithm would also fail because the reverberation spectrum is no longer spread, and it has a specific length in a specific frequency bin. NMF therefore recognizes this reverberation spectrum as the target echo. Owing to the lengthened block, the reverberation spectrum range is wider and the NMF requires more ranks. Therefore, this method is not a satisfactory solution.

To solve this problem, we adopt the modulo operation, which alters the LFM target echo continuously, regardless of its arrival time. Generally, the modulo operation involves finding the remainder after the division of one number by another. That is, numbers are wrapped around when attaining a certain value [24]. A similar concept is used in the phase unwrapping algorithm for speech signal processing. In this algorithm, the estimated phase is unwrapped to eliminate the discontinuity [25]. Motivated by this, we proposed a new technique to attach the target echo components in the spectrogram to their proper positions; hence, we named it the modulo operation. However, the proposed technique is different from the conventional concept because it focuses on the discontinuity in block processing. Fig. 6 shows that after the dechirping process, a signal in the LFM bandwidth is modified into a parallelogram. To maintain the target echo

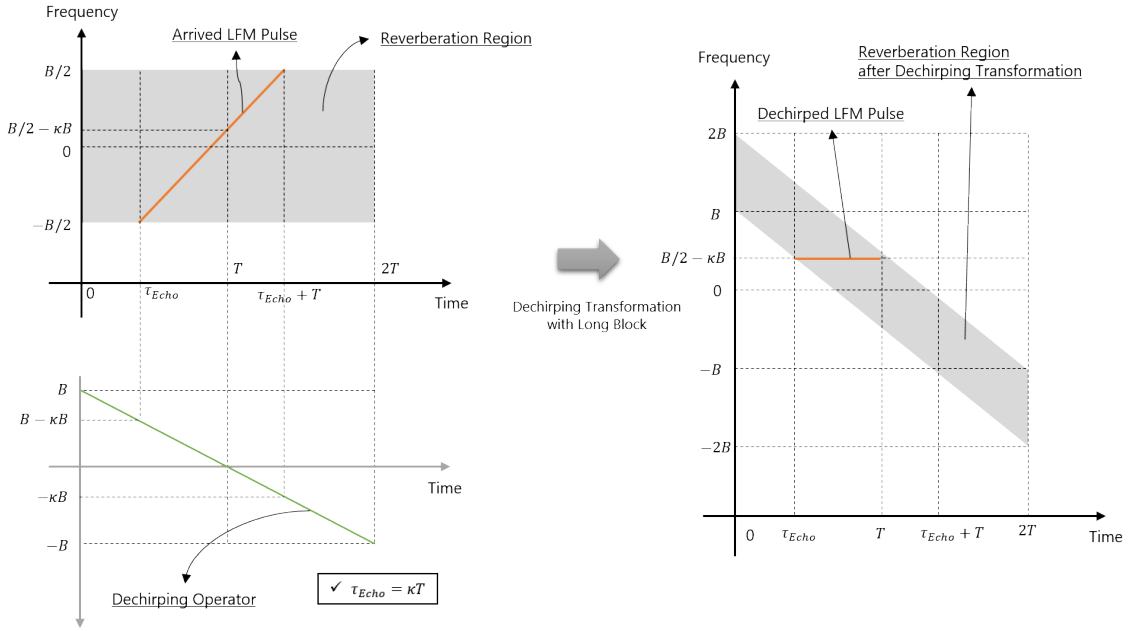

FIGURE 7. Problem of dechirping transformation when a block signal with double the length is applied at once.

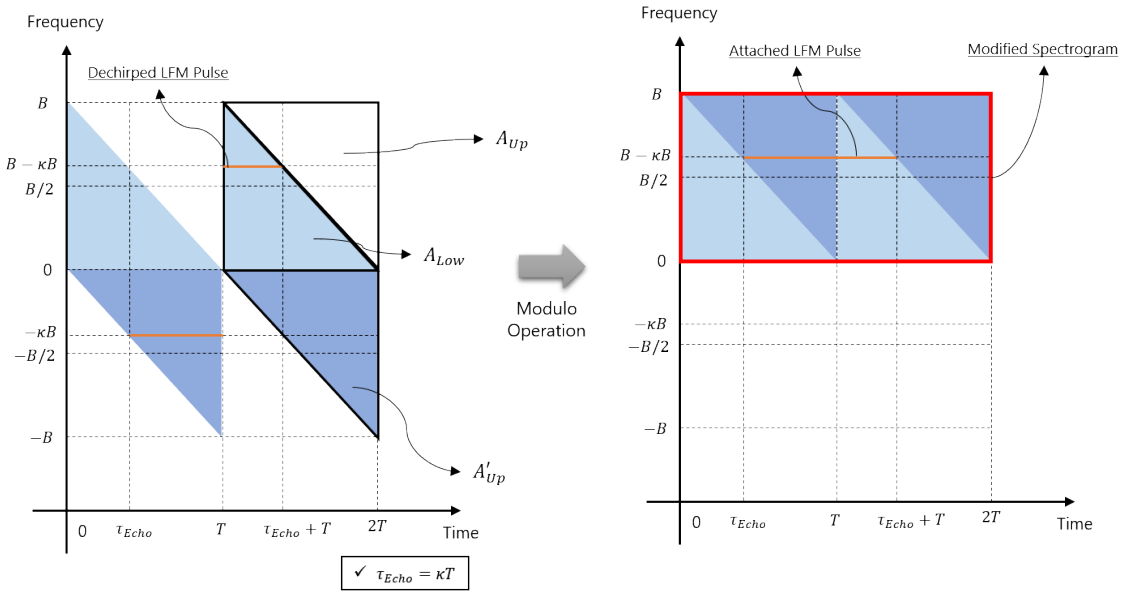

FIGURE 8. Modulo operation.

information, the lower triangle of this parallelogram needs to be attached to the right side of the upper triangular part. Through this modulo operation, the target echo signals in a different block are attached, and block processing problems are addressed. If we define $\mathbf{V}_{Dec,q}$ as a spectrogram of a dechirped signal $\mathbf{x}_{Dec,q}$, the modulo operation can be expressed as

$$\left[\mathbf{V}_{Mod,q}\right]_{(k,n)} = \begin{cases} \left[\mathbf{V}_{Dec,q}\right]_{(k,n)}, & (k,n) \in A_{Low} \\ \left[\mathbf{V}_{Dec,q}\right]_{(k-K_B,n)}, & (k,n) \in A_{Up}, \end{cases} \tag{20}$$

where $A_{Low} = \left\{(k,n)|0 \le k < -\frac{K_B}{M}n + K_B\right\}$, $A_{Up} = \left\{(k,n)|-\frac{K_B}{M}n + K_B < k \le K_B\right\}$ are set indicating the lower and upper triangular regions in the spectrogram, respectively. K_B is the number of bins corresponding to the bandwidth of the LFM pulse. After applying the modulo operation to each block, we attach these results as follows:

$$\mathbf{V}_{Mod} = \left[\mathbf{V}_{Mod,1} \vdots \cdots \vdots \mathbf{V}_{Mod,Q}\right]. \tag{21}$$

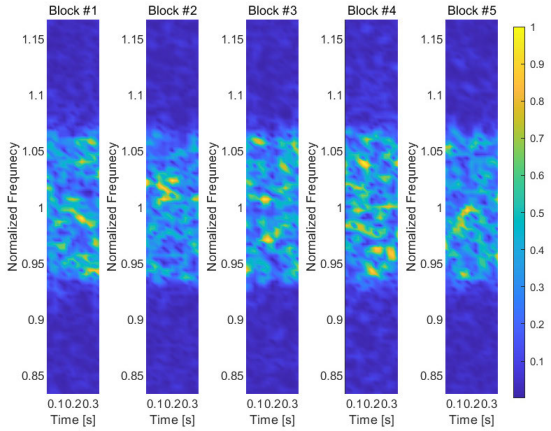

FIGURE 9. Spectrogram of block signals of simulation data.

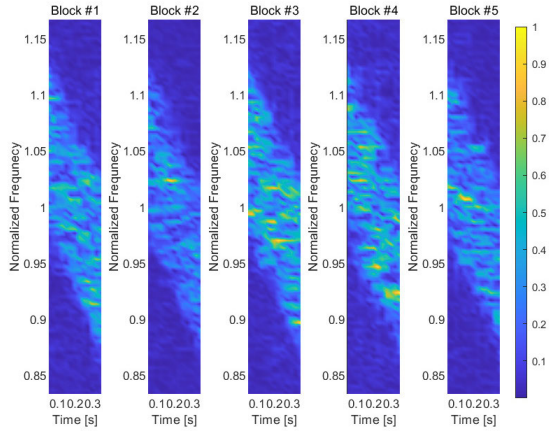

FIGURE 10. Spectrogram of dechirping-transformed block signal of simulation data.

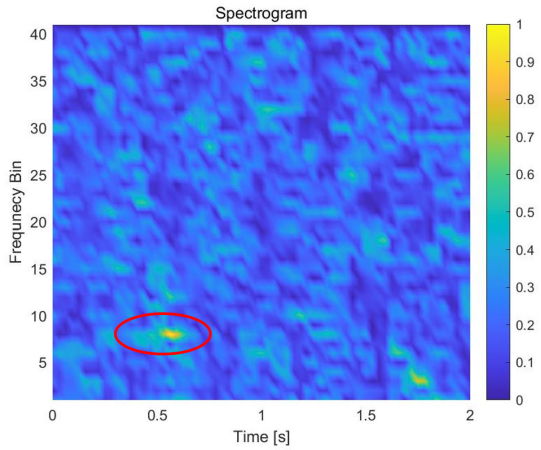

FIGURE 11. Modified spectrogram of simulation data.

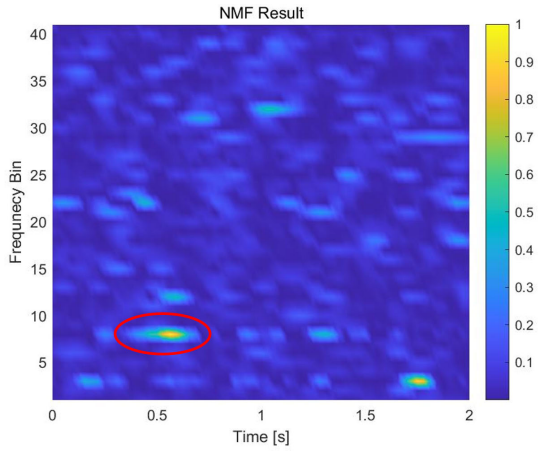

FIGURE 12. NMF results of simulation data.

Because the target echo can exist only in a frequency range from zero to bandwidth B, we remove the outer region before applying the NMF method. We can then apply the NMF method to this pre-processed spectrogram $\mathbf{V}_{Mod}$. Fig. 8 shows the modulo operation scheme in detail. The implemented NMF algorithm is the same as the algorithm used in CW sonars. The performance is improved via addition of sparse constraints, which are introduced subsequently.

C. ESTIMATING THE NMF BASIS MATRICES

The basic NMF model employs the same method as as Lee's NMF method, except that we use the pre-processed spectrogram in (21) as follows:

$$\mathbf{V}_{Mod} = \mathbf{W}_P\mathbf{H}_P + \mathbf{W}_R\mathbf{H}_R + \mathbf{E}. \tag{22}$$

To separate the target echo and the reverberation parts, we initialize and fix $\mathbf{W}_P$ as a Doppler-shifted frequency template for the pre-processed data, and we then estimate the matrices $\mathbf{H}_P$, $\mathbf{W}_R$, and $\mathbf{H}_R$ by applying the MU rules with KL divergence iteratively. To estimate the bases $\mathbf{H}_P$ properly, we apply some additional constraints, which can distinguish the target echo components, and then modify the update rules to utilize the sparsity of the target echo basis matrix. The constraints are the same as those of the conventional method [17]. However, the update rule to utilize the sparsity is an original contribution of this study.

To utilize the information of a target echo concentrated in a narrow frequency bin (strictly speaking, it does not represent real frequency because the dechirping transformation has been conducted), each basis of $\mathbf{W}_P$ is constrained to indicate the specific frequency bin, which relates to a specific arrival time of the transmitted LFM pulse. This can be implemented by one-hot encoding, indicating that only the elements of the column of $\mathbf{W}_P$ that have values for the specific elements in which the Doppler of the target is expected are used, while the remaining elements are set to zero. Therefore, $\mathbf{W}_P$ is set as

$$\mathbf{W}_P = \left[\mathbf{w}_{P,1}, \cdots, \mathbf{w}_{P,l}, \cdots, \mathbf{w}_{P,L_P}\right], \tag{23}$$

where $\mathbf{w}_{P,l} \in \mathbb{R}^{+}_{K\times 1}$ is the lth target echo frequency basis. $\mathbf{w}_{P,l}$ is expressed as

$$\mathbf{w}_{P,l} = [0, 0, \cdots, 1, \cdots, 0, 0]^T. \tag{24}$$

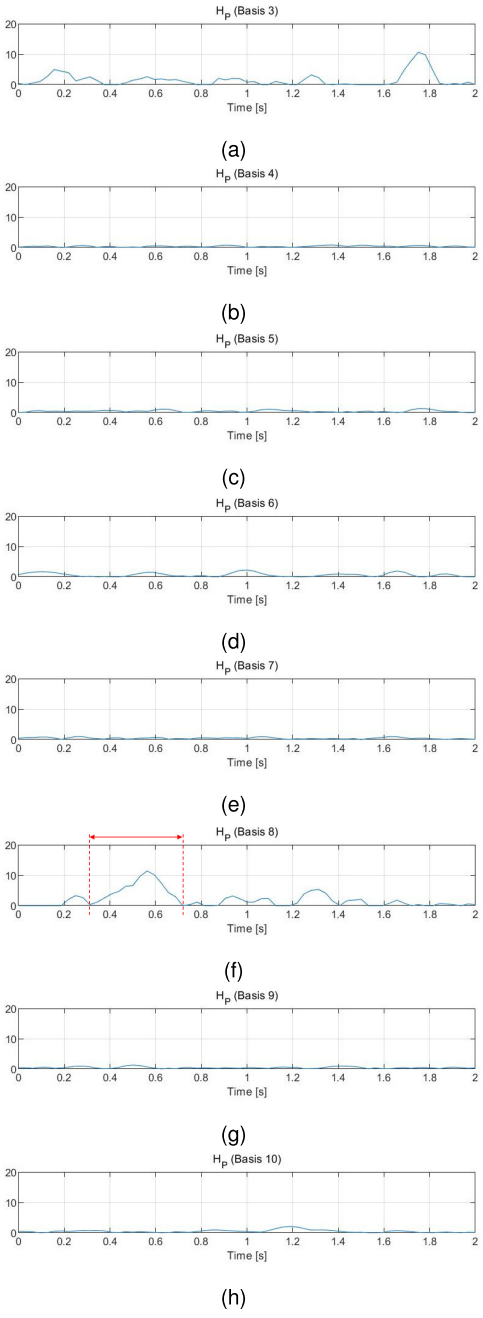

FIGURE 13. Estimated time basis of simulation data.

In this equation, the value 1 is placed at the specific frequency bin corresponding to the target echo arrival time. This structure is similar to the Doppler replica of the matched filter, which is used to verify all the hypotheses of the target Doppler to be detected.

To utilize information of the target echo that has continuous features in the time bin, $\mathbf{H}_P$ is estimated using a cost function expressed as

$$C(\mathbf{W}_P, \mathbf{H}_P) = C_{RE}(\mathbf{W}_P, \mathbf{H}_P) + \alpha C_{TC}(\mathbf{H}_P) + \beta C_{TLL}(\mathbf{H}_P), \tag{25}$$

TABLE 1. Summary of proposed algorithm.

1. Pre-processing:
1.1. Divide received signal in block units of length T_P
1.2. Apply dechirping transformation using (19)
1.3. Apply modulo operation using (20) and (21)

2. NMF method:
2.1. Initialize $\mathbf{W}_P$ using (23) and (24) and $\mathbf{W}_R$, $\mathbf{H}_P$, and $\mathbf{H}_R$ using uniform distribution with non-negative values
2.2. Update $\mathbf{W}_R$, $\mathbf{H}_P$, and $\mathbf{H}_R$ by (32), (33), and (34), respectively. These update equations are calculated iteratively until they converge
2.3. Estimate the target echo signal using (35)

3. Reconstruction of target echo signal:
3.1. Perform the demodulo operation using (36)
3.2. Perform inverse STFT and apply rechirping transformation using (37)
3.3 Finally, the target echo signal can be reconstructed using (38)

where $C_{RE}(\mathbf{W}_P, \mathbf{H}_P)$, $C_{TC}(\mathbf{H}_P)$, and $C_{TLL}(\mathbf{H}_P)$ are the cost of the reconstruction error (RE), the temporal continuity (TC), and the temporal length limitation (TLL), respectively.

The gradient of every cost is the weighted sum of the gradients of each cost:

$$\nabla_{\mathbf{H}_P} C = \nabla_{\mathbf{H}_P} C_{RE} + \alpha \nabla_{\mathbf{H}_P} C_{TC} + \beta \nabla_{\mathbf{H}_P} C_{TLL}, \tag{26}$$

where α and β are the weighting parameters for TC and TLL, respectively. Note that we omit the parentheses for convenience.

If we split this gradient into positive and negative terms, (26) is expressed as

$$\begin{aligned} \nabla_{\mathbf{H}_P} C = &\left(\nabla^+_{\mathbf{H}_P} C_{RE} - \nabla^-_{\mathbf{H}_P} C_{RE}\right) \\ &+ \alpha \left(\nabla^+_{\mathbf{H}_P} C_{TC} - \nabla^-_{\mathbf{H}_P} C_{TC}\right) \\ &+ \beta \left(\nabla^+_{\mathbf{H}_P} C_{TLL} - \nabla^-_{\mathbf{H}_P} C_{TLL}\right). \end{aligned} \tag{27}$$

Then, we can express the total gradient terms as

$$\nabla_{\mathbf{H}_P} C = \nabla^+_{\mathbf{H}_P} C - \nabla^-_{\mathbf{H}_P} C \tag{28}$$

where the positive terms $\nabla^+_{\mathbf{H}_P} C$ and the negative terms $\nabla^-_{\mathbf{H}_P} C$ are given by

$$\nabla^+_{\mathbf{H}_P} C = \nabla^+_{\mathbf{H}_P} C_{RE} + \alpha \nabla^+_{\mathbf{H}_P} C_{TC} + \beta \nabla^+_{\mathbf{H}_P} C_{TLL}, \tag{29}$$

$$\nabla^-_{\mathbf{H}_P} C = \nabla^-_{\mathbf{H}_P} C_{RE} + \alpha \nabla^-_{\mathbf{H}_P} C_{TC} + \beta \nabla^-_{\mathbf{H}_P} C_{TLL}, \tag{30}$$

respectively (see Appendix A for calculation of each term). Consequently, $\mathbf{H}_P$ can be estimated using (12) as

$$\mathbf{H}_P \leftarrow \mathbf{H}_P \circ \frac{\nabla^-_{\mathbf{H}_P} C}{\nabla^+_{\mathbf{H}_P} C}. \tag{31}$$

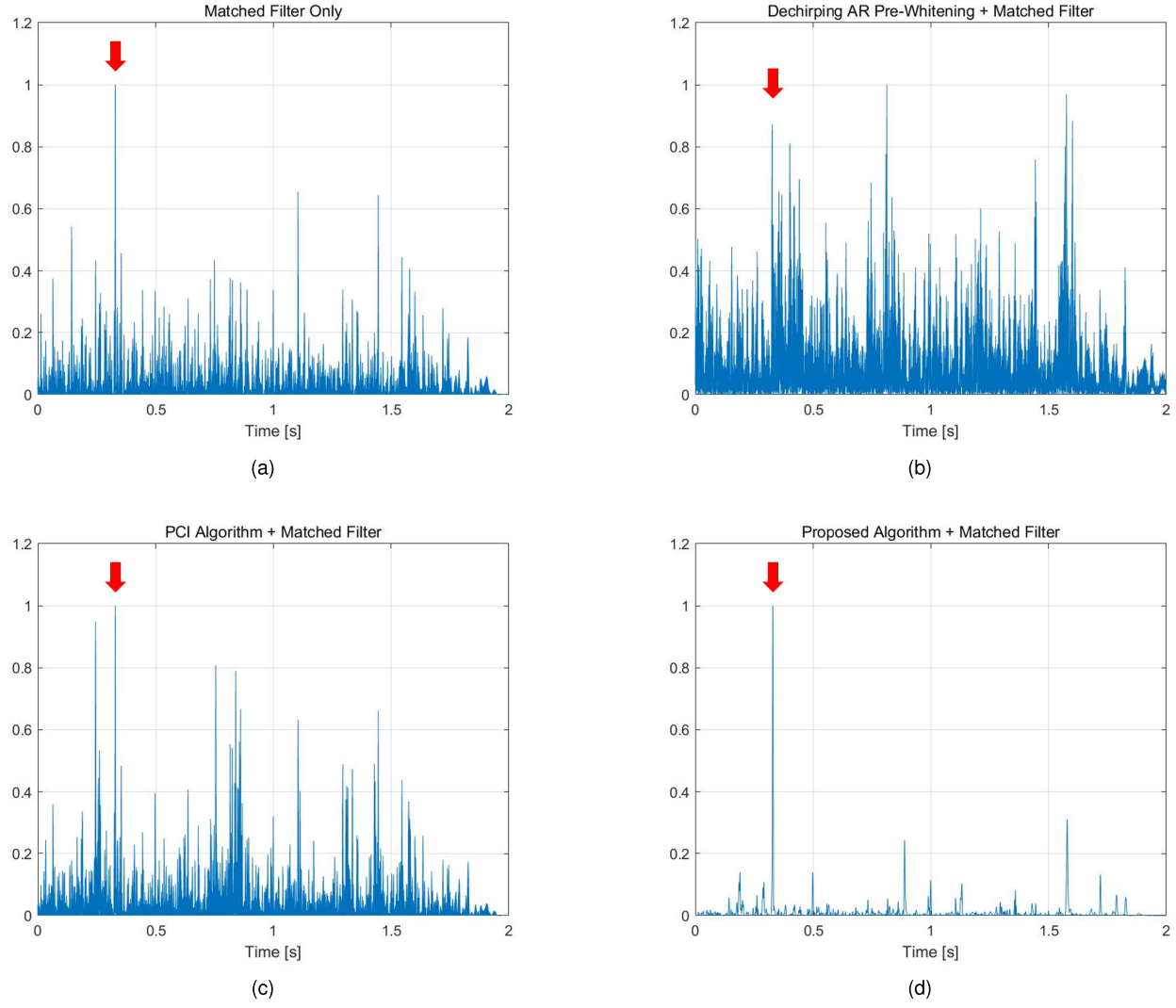

FIGURE 14. Comparison of matched filter results using (a) received signal, (b) output signal of dechirping AR pre-whitening, (c) output signal of PCI, and (d) output signal of the proposed algorithm with simulated data.

To improve the NMF algorithm performance, we modify it with sparse constraints. There are different techniques to handle sparse constraints; we have focused on estimating sparse channels using adaptive filters as we believe that it is suited for our study. Duttweiler proposed a proportionate normalized least mean square (PNLMS) algorithm, which is a variation of the least mean square (LMS) algorithm [26], [27]. In the PNLMS algorithm, each filter coefficient is updated by adjusting the step size in proportion to the estimated coefficient to utilize sparse information of the echo path channel. Recently, this concept has been extended to the arrival estimation algorithm [28]. Motivated by these studies, we propose sparse constraints on (31), which involve updating the echo time basis $\mathbf{H}_P$. Sparse update rules for $\mathbf{H}_P$ can be expressed as follows (see Appendix B):

$$\mathbf{H}_P \leftarrow (\mathbf{I}-\mathbf{D})\,\mathbf{H}_P + \mathbf{D}\frac{\nabla^-_{\mathbf{H}_P} C}{\nabla^+_{\mathbf{H}_P} C}\mathbf{H}_P, \tag{32}$$

where $\mathbf{I}$ is an identity matrix and $\nabla^+_{\mathbf{H}_P} C$ and $\nabla^-_{\mathbf{H}_P} C$ are the positive and the negative total gradient terms in (29) and (30), respectively. Moreover, $\mathbf{D}$ is a diagonal matrix, which consists of the normalized power of each basis vector.

Reverberation is assumed to contain a more fluctuating component with a constrained target echo part. Therefore, estimation of the reverberation basis is achieved via the MU rule without additional constraints as

$$\mathbf{W}_R \leftarrow \mathbf{W}_R \circ \frac{[\mathbf{V}/(\mathbf{WH})]\mathbf{H}_R}{\mathbf{1}_{K\times N}\mathbf{H}_R^T}, \tag{33}$$

$$\mathbf{H}_R \leftarrow \mathbf{H}_R \circ \frac{\mathbf{W}_R^T[\mathbf{V}/(\mathbf{WH})]}{\mathbf{W}_R^T\mathbf{1}_{K\times N}}. \tag{34}$$

The NMF algorithm is applied iteratively using (23), (32), (33), and (34) until it achieves convergence. After the NMF algorithm converges, the target echo information can be estimated by multiplying the matrices $\mathbf{W}_P$ and $\mathbf{H}_P$.

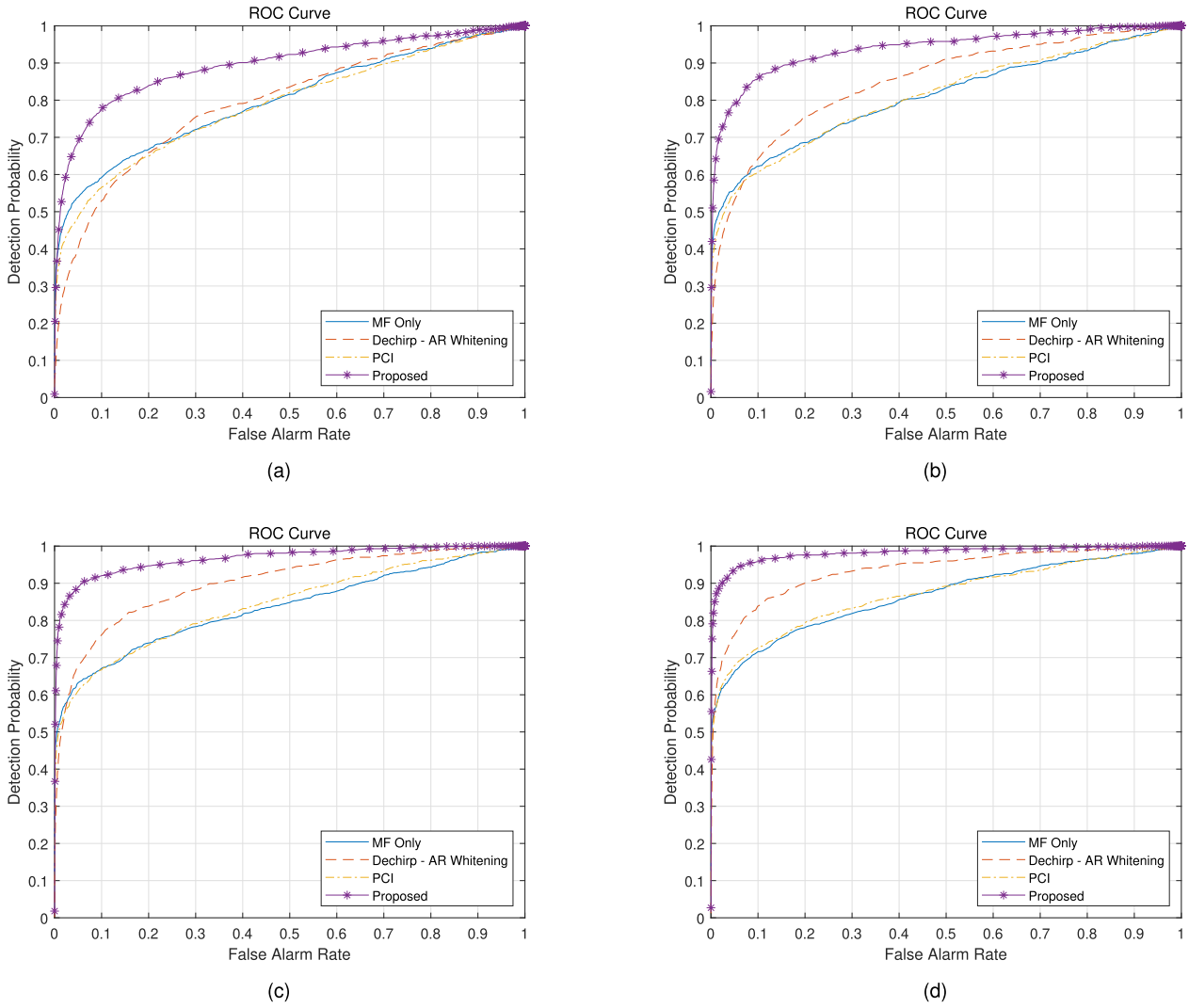

FIGURE 15. Analysis of receiver operating characteristics. This analysis was conducted at SRRs of (a) −12 dB, (b) −10 dB, (c) −8 dB, and (d) −6 dB.

The NMF results can be expressed as

$$\hat{\mathbf{V}} = \mathbf{W}_P \mathbf{H}_P. \tag{35}$$

D. RECONSTRUCTION OF TARGET ECHO SIGNAL

In order to apply additional signal processing such as a matched filter, the NMF results (35) need to be reconstructed to the time domain signal. Because two pre-processing steps are conducted, the inverse processing steps need to be applied in reverse order to reconstruct the target echo time signal. The demodulo operation (inverse operation of the modulo operation) is given by

$$\left[\mathbf{V}_{Dem,q}\right]_{(k,n)} = \begin{cases} \left[\hat{\mathbf{V}}_q\right]_{(k,n)}, & (k,n) \in A_{Low} \\ \left[\hat{\mathbf{V}}_q\right]_{(k+K_B,n)}, & (k,n) \in A'_{Up} \\ 0, & otherwise \end{cases} \tag{36}$$

where $A'_{Up} = \left\{(k,n) | -\frac{K_B}{M} n < k \leq 0\right\}$ and $\hat{\mathbf{V}}_q$ are the qth block of the NMF results using (35). Because we eliminate the noise, this region is filled with zeros.

Thereafter, the rechirping transformation (inverse transformation of the dechirping transformation) is performed. Before performing the rechirping transformation, we perform an inverse STFT, as this transformation is performed in the time domain. Note that the result of the STFT is a complex value. Because the NMF algorithm uses only the magnitude part to reconstruct the target echo signal from the estimated non-negative matrix, we require the phase information. This phase information can be obtained from the STFT results of the original input signal [20].

If we define $\mathbf{x}_{Dem,q}$ as the inverse STFT signal for $\mathbf{V}_{Dem,m}$, the rechirping transformation can be expressed as

$$\hat{\mathbf{x}}_q = \mathbf{x}_{Dem,q} \circ \mathbf{g}^*, \tag{37}$$

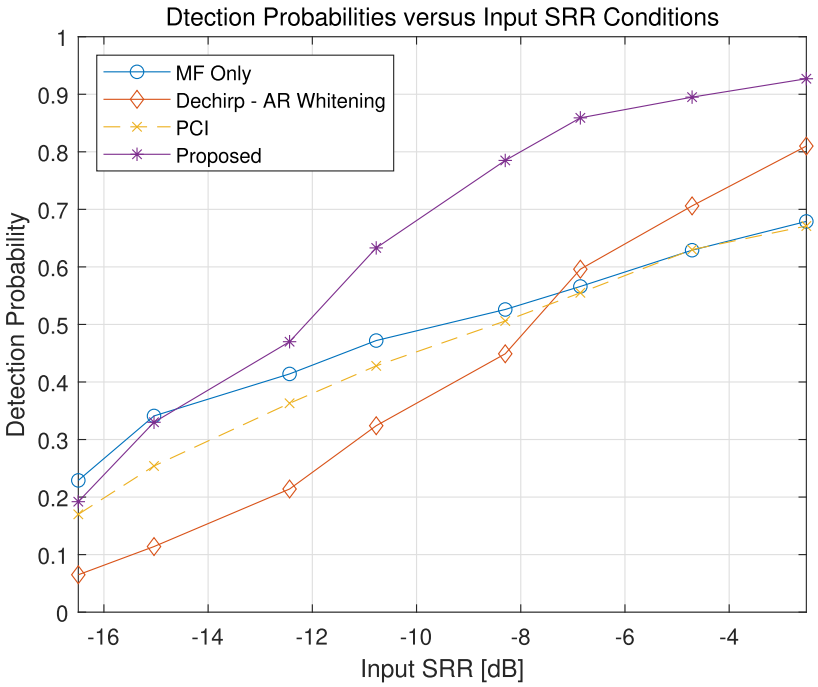

FIGURE 16. Detection probabilities versus SRR at false alarm rate of 1%.

where $*$ indicates the element-wise conjugate. Since the rechirping transformation is the inverse of the dechirping transformation, $\mathbf{g}^*$, which represents the inverse sweep rate, indicates rechirping vector.

In summary, a reconstructed target echo signal can be obtained by attaching each rechirped block signal as follows:

$$\hat{\mathbf{x}} = \left[\hat{\mathbf{x}}_1^T \cdots \hat{\mathbf{x}}_q^T \cdots \hat{\mathbf{x}}_Q^T\right]^T. \tag{38}$$

We summarize the proposed LFM reverberation suppression algorithm in Table 1.

IV. SIMULATION

To evaluate the proposed LFM reverberation suppression method, we simulated a received echo signal using reverberation environments with a 0.4 s LFM pulse. In the simulation, the LFM reverberation was synthesized on the basis of (5). To simulate the reverberation, we synthesized 3000 zero-Doppler LFM signals. The arrival time was assumed to have a uniform distribution with a duration of 2 s, and the attenuation factor was set to a normal distribution with a mean of 1 and standard deviation of 0.1.

To implement the NMF method, we applied the dechirping transformation, STFT, and modulo operation consecutively, as explained in Section III. The processing block length was equal to the pulse length. STFT was performed with a 0.1 s Hamming window and a 75% overlap. The NMF basis number L was 410, of which the target echo part L_P and the reverberation part L_R were 41 and 369, respectively. The TC weighting parameter α, TLL weighting parameter β, and expected echo length l_T were set to 10, 1, and 1.5 s, respectively.

The spectrogram of the simulated reverberation environment in the block unit is shown in Fig. 9, and the spectrogram of its dechirping transformation is shown in Fig. 10. The modified spectrogram obtained after the modulo operation is shown in Fig. 11. In this example, the target was set to arrive at 0.33 s with a Doppler of 0.3 m/s. The signal-to-reverberation ratio (SRR) was set to -12 dB, which represents a harsh target detection environment. A red ellipse emphasizes the target echo component, which is difficult to recognize because it is hidden in the reverberation component. However, we can observe in Fig. 12 that the NMF algorithm suppresses the reverberation components, and the target is enhanced when compared to that in Fig. 11. Fig. 13 shows an example of the estimated target echo time basis from the third to tenth bases. On the eighth basis, we can observe a significant component between 0.3 to 0.7 s, whereas the components of the other bases are relatively small.

We compared the detection performance of the proposed algorithm with the no reverberation suppression algorithm, the dechirping AR pre-whitening algorithm, and the PCI algorithm. In the simulation, we used a normalized matched filter as detector [29]. The normalized matched filter results can be calculated as

$$\chi(t) = \frac{\int x(t)s_p(t)\,dt}{\sqrt{\int x^2(t)\,dt \int s_p^2(t)\,dt}}. \tag{39}$$

To calculate the normalized matched filter results, we used only a zero-Doppler replica because the LFM pulse is

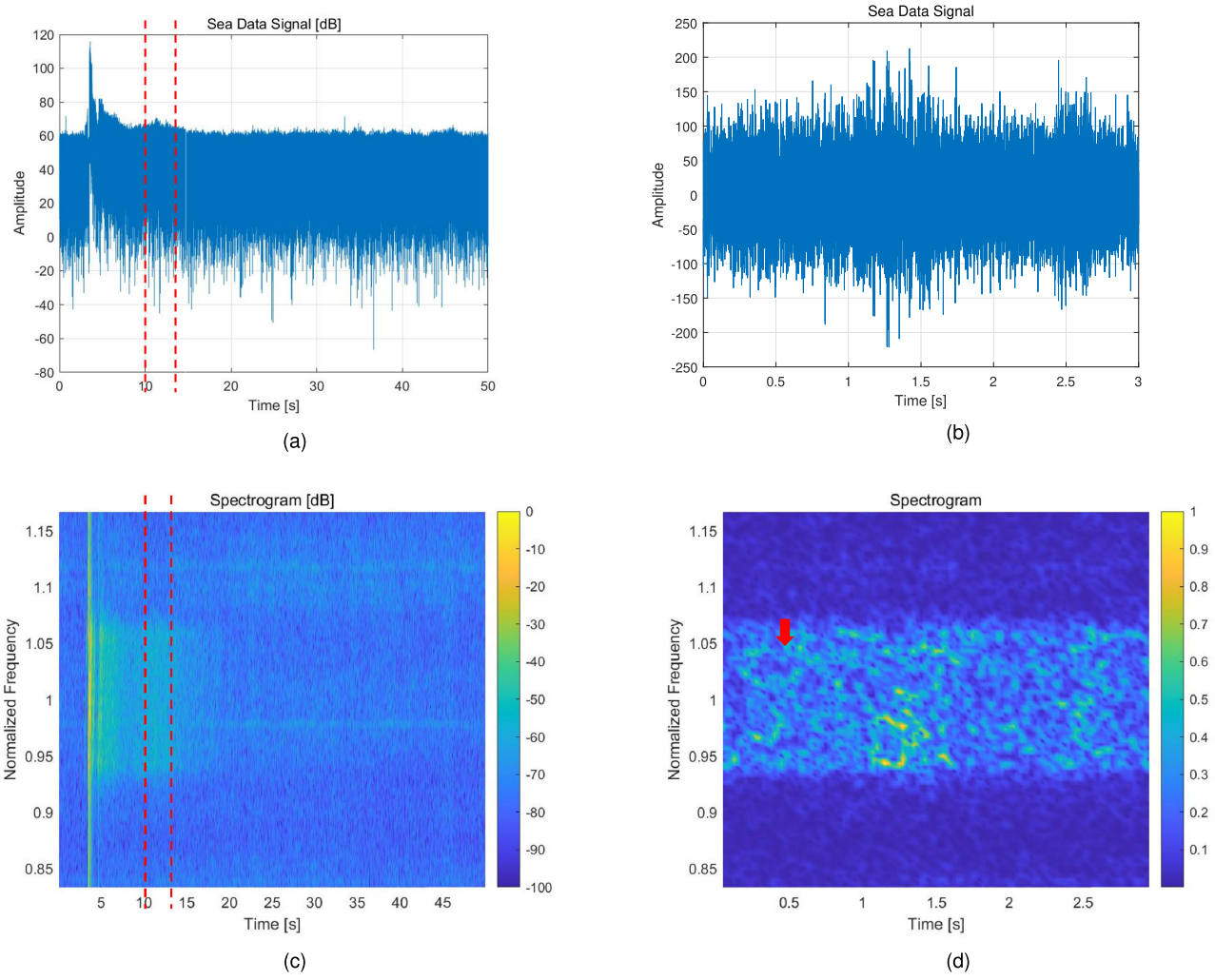

FIGURE 17. Sea experiment data with (a) time signal (whole duty cycle, dB scale), (b) time signal (reverberation region, linear scale), (c) spectrogram (whole duty cycle, dB scale), and (d) spectrogram (reverberation region, linear scale).

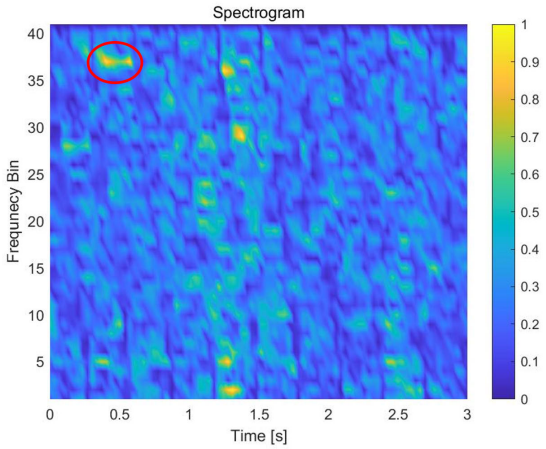

FIGURE 18. Modified spectrogram of the sea experiment data.

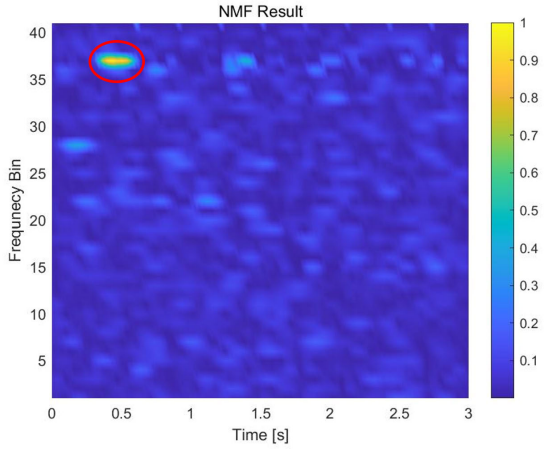

FIGURE 19. NMF results of the sea experiment data.

Doppler insensitive. The order for the AR model was set to 20, and it had the optimal condition in which the reference signal is exactly the same as the reverberation signal. The PCI algorithm also had the optimal condition in which the threshold was set assuming the power of reverberation was known.

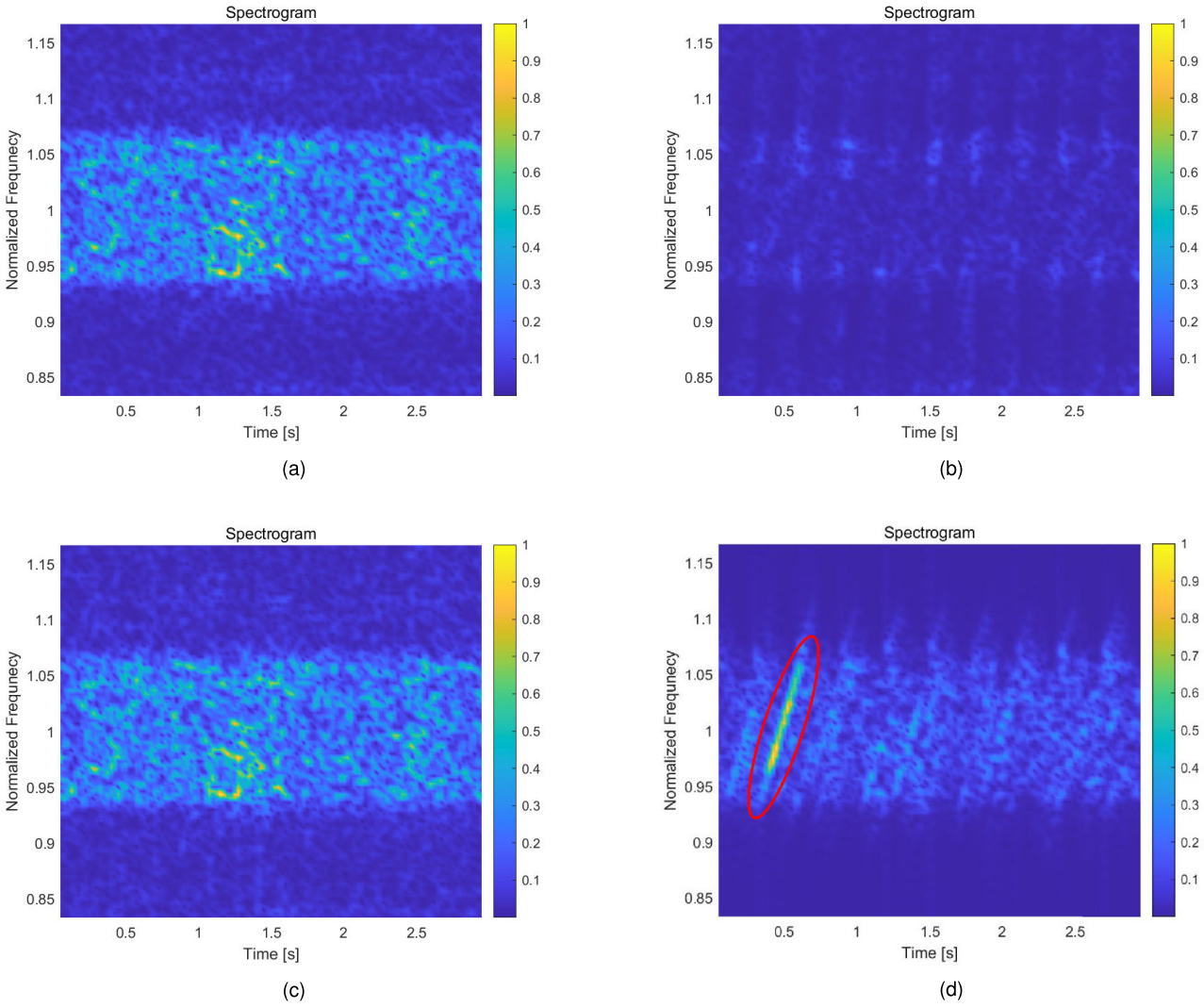

FIGURE 20. Spectrogram comparison of (a) received signal, (b) output signal of dechirping AR pre-whitening, (c) output signal of PCI, and (d) output signal of the proposed algorithm with the sea experiment data.

Fig. 14 shows the matched filter results at SRR −12 dB using the reconstructed target echo signals. We can observe the target echo peaks when the proposed algorithm is applied because reverberation is considerably suppressed. We can also observe that the target echo peaks are very narrow in the time domain owing to the time compression ability of the LFM pulse. Meanwhile, other results show many interfering peaks caused by reverberation. To compare the simulation results, the output SRR, echo peak to maximum sidelobe peak ratio (PMPR) of the matched filter, and echo peak to average sidelobe peak ratio (PAPR) of the matched filter were calculated. The output SRR was calculated by the energy ratio of the target (ground truth) signal and the errors between the estimated and the target signals. The PMPR and PAPR were calculated as

$$\text{PMPR} = 10\log\frac{|\chi(\tau_e)|^2}{\max_{t\in I}|\chi(t)|^2} \tag{40}$$

$$\text{PAPR} = 10\log\frac{|\chi(\tau_e)|^2}{\frac{1}{|I|}\int_{t\in I}|\chi(t)|^2}, \tag{41}$$

where I is the interval from 0 to the duration of the simulation except for the location of the target echo peak and $|I|$ is the length of the interval I. The calculated results are presented in Table 2. Because the SRR condition of simulation (−12 dB) is not suitable for comparison of the algorithms, AR prewhitening and PCI failed to work properly. Meanwhile, the proposed algorithm worked well and provided SRR, PMPR, and PAPR enhancements of approximately 13 dB, 3.2 dB, and 4.6 dB, respectively, for the same condition. For the quantitative analysis of detection performance, we calculated the probabilities of detection and false alarm rate by performing 1000 Monte Carlo simulations per SRR. Fig. 15 shows the receiver operating characteristic (ROC) curve with SRRs of −12 dB, −10 dB, −8 dB, and −6 dB. The matched filter results show that the proposed algorithm has a superior detection performance compared to the other

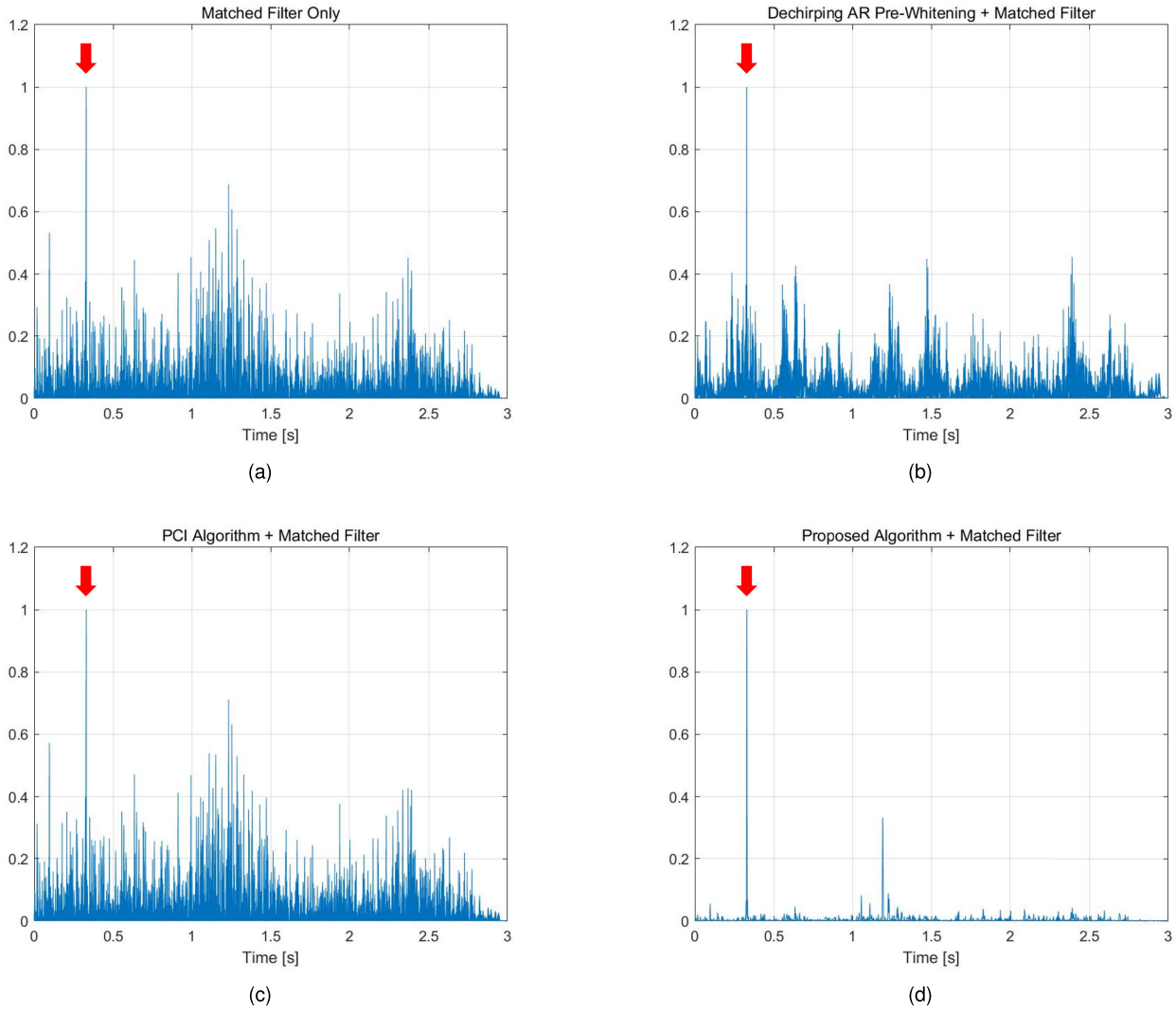

FIGURE 21. Comparison of matched filter results using (a) received signal, (b) output signal of dechirping AR pre-whitening, (c) output signal of PCI, and (d) output signal of the proposed algorithm with the sea experiment data.

TABLE 2. Performance comparison with simulated data (input SRR = −12 dB).

	output SRR [dB]	PMPR [dB]	PAPR [dB]
Received signal	-12.37	1.83	15.16
Output signal of dechirping AR pre-whitening	-14.07	-0.59	9.62
Output signal of PCI	-11.55	0.22	14.24
Output signal of the proposed algorithm	0.64	5.09	19.75

methods in all SRR conditions. Fig. 16 shows the detection probabilities with respect to SRR conditions at a false alarm rate of 1%. From this graph, we can also see that the detection performance of the proposed algorithm is superior compared to that of other methods.

V. SEA EXPERIMENT DATA ANALYSIS

We also tested the proposed LFM reverberation suppression algorithm with sea data experiments, which were conducted at the Eastern Sea of Pohang, Republic of Korea. In these experiments, an LFM pulse with a pulse length of 0.3 s was used, and an echo repeater was used to generate the target echo signal. However, the received echo repeater signal was located in the noise-limited region, and the performance of the proposed algorithm in such regions was not considered. Therefore, we cut out the echo repeater signal and relocated it at the time which included the reverberation-limited region. The target was set to arrive at 0.33 s, and its Doppler was

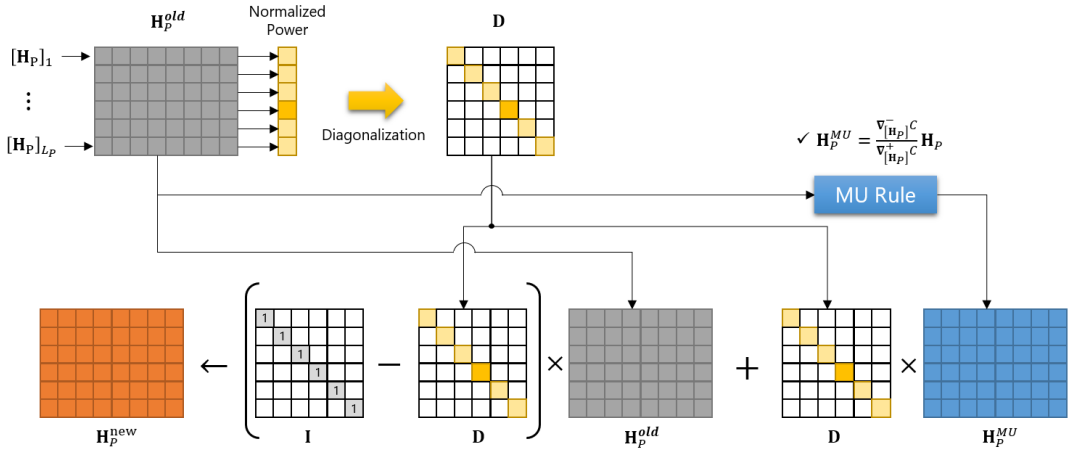

FIGURE 22. Scheme of the proposed sparse constraints.

estimated as 0.3 m/s. Note that this time axis is not synchronized with the transmission time. Therefore, the arrival time of 0.33 s does not imply 0.33 s after transmission. Because the pulse length differs from that of the simulation, we used a 0.3 s block length, although the parameters to perform the proposed algorithm are the same as in the simulation.

Figs. 17 (a) and (b) show the recorded time signals of the sea experiments, and Figs. 17 (c) and (d) show its spectrogram. Note that Figs. 17 (a) and (c) are displayed as a dB scale for convenience. In these figures, we can observe the strong direct blast signal in the early part of this duty cycle and the decrease in the power of the reverberation until it remains constant at 15 s. The dotted red line in the figures indicates the region of 10–13 s, which relates to the reverberation parts, thus verifying the proposed algorithm. These regions are shown in Figs. 17 (b) and (d). That is, these are expansions of the reverberation-limited region. The red arrow in Fig. 17 (d) indicates where the target echo is located. Fig. 3 and Fig. 17 (d) show very similar characteristics. This confirms that the assumed reverberation environment is valid in practice.

Fig. 18 and Fig. 19 show a modified spectrogram and the NMF results of the sea experiment data, respectively. Similar to the simulation results, the proposed algorithm suppresses the reverberation and emphasizes the target echo. Fig. 20 and Fig. 21 show the spectrogram and the matched filter results of the reconstructed target echo signals, respectively. In the spectrogram of the proposed algorithm, we can observe that the target component (represented by the ellipse) is located at the true echo time delay (0.33 s). However, this component is difficult to locate in the other results. The matched filter results indicate that, unlike the others, the proposed algorithm effectively removes reverberation, confirming that the target is clearly detected. These figures illustrate that the proposed algorithm suppresses the reverberation component effectively in real sea environments.

VI. CONCLUSION

In this study, a novel LFM reverberation suppression algorithm was proposed. The proposed algorithm is based on the NMF method. Because LFM reverberation differs from CW reverberation, we adopted two pre-processing steps. Specifically, the dechirping transformation and the modulo operation are used. The dechirping transformation is used to transform the LFM target echo into a horizontal line in the spectrogram, and the modulo operation is used to prevent loss of the target echo information by block processing. In addition, we modified the NMF method by adding sparse constraints on the estimation of the target echo time basis to improve the NMF performance.

To confirm the proposed LFM reverberation suppression algorithm, we conducted computer simulations and analyses of sea experimental data. The simulation results show that the proposed algorithm demonstrated a considerable ability to suppress reverberation. Furthermore, we compared the detection performance of the proposed algorithm with that of conventional LFM reverberation suppression algorithms, dechirping AR whitening, and the PCI algorithm. In the quantitative evaluation, we confirmed that output SRR, PMPR, and PAPR are improved by 13 dB, 3.2 dB, and 4.6 dB, respectively, when input SRR is -12 dB. Through the analysis of ROC curves and detection probability versus an SRR condition graph, we statistically verified that the performance of the proposed algorithm is superior compared to that of other algorithms when it converges in valid SRR conditions. To clearly verify the performance of the proposed algorithm, sea experiment data were used. In the experiment, the proposed algorithm efficiently suppressed the real LFM reverberation, thereby confirming that target detection performance was improved. In summary, the proposed algorithm has demonstrated good performance in simulations and can also be applied in practical LFM sonar systems.

APPENDIX A
REVIEW OF GRADIENTS OF CONSTRAINTS IN THE NMF METHOD

The cost function is composed of three parts. The reconstruction error (RE) C_{RE} is defined by the KL divergence, which is generally used in the NMF algorithm, and its gradient terms are given by [19]

$$\nabla^{+}_{\mathbf{H}_P} C_{RE} = \mathbf{W}_P^T \mathbf{1}_{K\times N}, \tag{42}$$

$$\nabla^{-}_{\mathbf{H}_P} C_{RE} = \mathbf{W}_P^T \frac{\mathbf{V}}{\mathbf{WH}}. \tag{43}$$

The temporal continuity (TC) is utilized as the time continuity characteristic of the echo signal and its gradient terms are given by [20]

$$\nabla^{+}_{\mathbf{H}_P} C_{TC} = \frac{4\,N\mathbf{H}_P}{\mathbf{H}_P^2 \mathbf{1}_{N\times N}}, \tag{44}$$

$$\nabla^{-}_{\mathbf{H}_P} C_{TC} = 2N \frac{\mathbf{H}_{P\to 1} - \mathbf{H}_{P\leftarrow 1}}{\mathbf{H}_P^2 \mathbf{1}_{N\times N}} + \frac{2N\mathbf{H}_P \circ \left[(\mathbf{H}_P - \mathbf{H}_{P\to 1})^2\, \mathbf{1}_{N\times N}\right]}{\left(\mathbf{H}_P^2 \mathbf{1}_{N\times N}\right)^2}, \tag{45}$$

where $\mathbf{H}_{P\leftarrow 1}$, $\mathbf{H}_{P\leftarrow 1}$ are versions of $\mathbf{H}_P$ shifted one column to the left and right, respectively, and $\mathbf{1}_{N\times N}$ is an $N \times N$ matrix whose elements are all one. In addition, $\mathbf{A}^2$ indicates an element-wise square of matrix $\mathbf{A}$.

The temporal length limitation (TLL) is utilized as the limited duration characteristic of the echo signal and its gradient terms are given by [17]

$$\left[\nabla^{+}_{\mathbf{H}_P} C_{TLL}\right]_{(r,n)} = \sum_{m=n}^{n+l_T-1} \left(\frac{e^{\left[\bar{\mathbf{H}}_P\right]_{(r,m)}}}{\sum_{i=1}^{N} e^{\left[\bar{\mathbf{H}}_P\right]_{(r,i)}}} \right)^2, \tag{46}$$

$$\left[\nabla^{-}_{\mathbf{H}_P} C_{TLL}\right]_{(r,n)} = \sum_{m=n}^{n+l_T-1} \left(\frac{e^{\left[\bar{\mathbf{H}}_P\right]_{(r,m)}}}{\sum_{i=1}^{N} e^{\left[\bar{\mathbf{H}}_P\right]_{(r,i)}}} \right), \tag{47}$$

where $[\mathbf{A}]_{(r,n)}$ is the (r,n) element of matrix $\mathbf{A}$ and l_T is the expected target echo length. $\left[\bar{\mathbf{H}}_P\right]_{(r,n)}$ is calculated by the moving sum of each target echo time basis, i.e., rows of $\mathbf{H}_P$. It is expressed as

$$\left[\bar{\mathbf{H}}_P\right]_{(r,n)} = \sum_{m=n-l_T+1}^{n} [\mathbf{H}_P]_{(r,m)}. \tag{48}$$

APPENDIX B
SPARSE UPDATE RULE FOR THE ECHO TIME BASIS MATRIX

The originally used MU rule in (31) is a modification of the element-wise gradient descent algorithm, which can be expressed as follows:

$$[\mathbf{H}_P]_{(r,n)} \leftarrow [\mathbf{H}_P]_{(r,n)} - \eta_{(r,n)} \left(\nabla^{+}_{[\mathbf{H}_P]_{(r,n)}} C - \nabla^{-}_{[\mathbf{H}_P]_{(r,n)}} C \right), \tag{49}$$

where $\eta_{(r,n)}$ is the step size parameter for update and $\nabla^{+}_{[\mathbf{H}_P]_{(r,n)}} C$ and $\nabla^{-}_{[\mathbf{H}_P]_{(r,n)}} C$ are the element-wise positive and negative parts of the gradient, which have non-negative values. Generally, $\eta_{(r,n)}$ is set to a small positive scalar value, but if we replace it as $\eta_{(r,n)} = [\mathbf{H}_P]_{(r,n)} / \nabla^{+}_{[\mathbf{H}_P]_{(r,n)}} C$, we can obtain (31). Using this process, if we control the step size appropriately, we can reflect our intention.

Therefore, to apply sparse constraints, we set the step size parameter proportional to the power of each basis vector as follows:

$$\eta_{(r,n)} = d_r \frac{[\mathbf{H}_P]_{(r,n)}}{\nabla^{+}_{[\mathbf{H}_P]_{(r,n)}} C}, \tag{50}$$

where d_r is the normalized power of each basis vector, which can be expressed as

$$d_r = \frac{\| [\mathbf{H}_P]_r \|_2}{\max\left(\| [\mathbf{H}_P]_1 \|_2, \cdots, \| [\mathbf{H}_P]_{L_P} \|_2 \right)}, \tag{51}$$

where $[\mathbf{H}_P]_r$ is the rth row vector of $\mathbf{H}_P$ and $\| \cdot \|_2$ indicates the diagonal matrix, l_2-norm. Note that we constrain each power of the echo time basis and not each element of $\mathbf{H}_P$. If we substitute (49) into (50), it yields the new element-wise update rule as follows:

$$[\mathbf{H}_P]_{(r,n)} \leftarrow (1 - d_r)\, [\mathbf{H}_P]_{(r,n)} + d_r \frac{\nabla^{-}_{[\mathbf{H}_P]_{(r,n)}} C}{\nabla^{+}_{[\mathbf{H}_P]_{(r,n)}} C} [\mathbf{H}_P]_{(r,n)}. \tag{52}$$

If we formulate these element-wise update rules in a matrix form, we can replace equation (31) as follows:

$$\mathbf{H}_P \leftarrow (\mathbf{I} - \mathbf{D})\, \mathbf{H}_P + \mathbf{D} \frac{\nabla^{-}_{\mathbf{H}_P} C}{\nabla^{+}_{\mathbf{H}_P} C} \mathbf{H}_P, \tag{53}$$

where $\mathbf{I}$ is an identity matrix and $\nabla^{+}_{\mathbf{H}_P} C$ and $\nabla^{-}_{\mathbf{H}_P} C$ are positive and negative total gradient terms in (29) and (30), respectively. $\mathbf{D}$ is a diagonal matrix, which consists of the normalized power of each basis vector and can be expressed as follows:

$$\mathbf{D} = \mathrm{diag}\left(d_1, \cdots, d_{L_P}\right), \tag{54}$$

where diag($\cdot$) indicates a diagonal matrix. Fig. 22 shows the scheme of the proposed sparse constraints in detail.

REFERENCES

[1] R. J. Urick, *Principles of Underwater Sound for Engineers*. New York, NY, USA: McGraw-Hill, 1967.
[2] D. A. Abraham, *Underwater Acoustic Signal Processing: Modeling, Detection, and Estimation*. Cham, Switzerland: Springer, 2019.
[3] R. O. Nielsen, *Sonar Signal Processing*. Norwood, MA, USA: Artech House, 1991.
[4] A. D. Waite and A. Waite, *Sonar for Practising Engineers*, vol. 3. New York, NY, USA: Wiley, 2002.
[5] T. Collins and P. Atkins, "Doppler-sensitive active sonar pulse designs for reverberation processing," *IEE Proc. Radar, Sonar Navigat.*, vol. 145, no. 6, pp. 347–353, Dec. 1998.
[6] T. Collins, "Active sonar pulse design," Ph.D. dissertation, School Electron. Elect. Eng., Univ. Birmingham, Birmingham, U.K., 1996.
[7] Y. Doisy, L. Deruaz, S. P. van IJsselmuide, S. P. Beerens, and R. Been, "Reverberation suppression using wideband Doppler-sensitive pulses," *IEEE J. Ocean. Eng.*, vol. 33, no. 4, pp. 419–433, Oct. 2008.

[8] Y. Doisy, L. Deruaz, B. Prunel, R. Been, S. Beerens, and S. V. IJsselmuide, "Sonar waveforms for reverberation rejection—Part III: More experimental results," in *Proc. UDT Eur. Conf. Undersea Defence Technol.*, London, U.K., Jun. 2000, pp. 27–29.
[9] S. V. Ijsselmuide, L. Deruaz, R. Been, Y. Doisy, and S. Beerens, "Sonar waveforms for reverberation rejection—Part IV: Adaptive processing," in *Proc. Undersea Defense Technol. (UDT) Eur.* Swanley, U.K.: Nexus Media, Ltd., 2002.
[10] D. A. Hague, "The generalized sinusoidal frequency modulated waveform for active sonar systems," 2018, *arXiv:1809.11009*. [Online]. Available: http://arxiv.org/abs/1809.11009
[11] D. A. Hague and J. R. Buck, "The generalized sinusoidal frequency modulated waveform for high duty cycle active sonar," in *Proc. 48th Asilomar Conf. Signals, Syst. Comput.*, Nov. 2014, pp. 148–152.
[12] S. Kay and J. Salisbury, "Improved active sonar detection using autoregressive prewhiteners," *J. Acoust. Soc. Amer.*, vol. 87, no. 4, pp. 1603–1611, Apr. 1990.
[13] V. Carmillet, P.-O. Amblard, and G. Jourdain, "Detection of phase- or frequency-modulated signals in reverberation noise," *J. Acoust. Soc. Amer.*, vol. 105, no. 6, pp. 3375–3389, Jun. 1999.
[14] B. W. Choi, E. H. Bae, J. S. Kim, and K. K. Lee, "Improved prewhitening method for linear frequency modulation reverberation using dechirping transformation," *J. Acoust. Soc. Amer.*, vol. 123, no. 3, pp. EL21–EL25, Mar. 2008.
[15] G. Ginolhac and G. Jourdain, "'Principal component inverse' algorithm for detection in the presence of reverberation," *IEEE J. Ocean. Eng.*, vol. 27, no. 2, pp. 310–321, Apr. 2002.
[16] W. Li, Q. Zhang, X. Ma, and C. Hou, "Active sonar detection in reverberation via signal subspace extraction algorithm," *EURASIP J. Wireless Commun. Netw.*, vol. 2010, no. 1, pp. 1–10, Dec. 2010.
[17] S. Lee and J.-S. Lim, "Reverberation suppression using non-negative matrix factorization to detect low-Doppler target with continuous wave active sonar," *EURASIP J. Adv. Signal Process.*, vol. 2019, no. 1, p. 11, Dec. 2019.
[18] D. D. Lee and H. S. Seung, "Learning the parts of objects by non-negative matrix factorization," *Nature*, vol. 401, no. 6755, p. 788, 1999.
[19] D. D. Lee and H. S. Seung, "Algorithms for non-negative matrix factorization," in *Proc. Adv. Neural Inf. Process. Syst.*, 2001, pp. 556–562.
[20] T. Virtanen, "Monaural sound source separation by nonnegative matrix factorization with temporal continuity and sparseness criteria," *IEEE Trans. Audio, Speech Lang. Process.*, vol. 15, no. 3, pp. 1066–1074, Mar. 2007.
[21] M. Barlaud, J. M. Bruneau, and M. Le Dard, "Sonar reverberation synthesis using nonstationary autoregressive modeling," in *Proc. Int. Conf. Acoust., Speech, Signal Process.*, Apr. 1990, pp. 2935–2938.
[22] J. Luby and D. Lytle, "Autoregressive modeling of nonstationary multibeam sonar reverberation," *IEEE J. Ocean. Eng.*, vol. OE-12, no. 1, pp. 116–129, Jan. 1987.
[23] S. K. Mitra and Y. Kuo, *Digital Signal Processing: A Computer-Based Approach*, vol. 2. New York, NY, USA: McGraw-Hill, 2006.
[24] T. H. Cormen, C. E. Leiserson, R. L. Rivest, and C. Stein, *Introduction to Algorithms*. Cambridge, MA, USA: MIT Press, 2009.
[25] T. F. Quatieri, *Discrete-Time Speech Signal Processing: Principles and Practice*. London, U.K.: Pearson, 2006.
[26] D. L. Duttweiler, "Proportionate normalized least-mean-squares adaptation in echo cancelers," *IEEE Trans. Speech Audio Process.*, vol. 8, no. 5, pp. 508–518, Sep. 2000.
[27] J. Benesty and S. L. Gay, "An improved PNLMS algorithm," in *Proc. IEEE Int. Conf. Acoust. Speech Signal Process.*, May 2002, pp. II-1881–II-1884.
[28] S. Lee, "Estimation of the acoustic time delay of arrival by adaptive eigenvalue decomposition with a proportionate step-size control and direct-path constraint," *IEICE Trans. Fundamentals Electron., Commun. Comput. Sci.*, vol. 99, no. 8, pp. 1622–1627, 2016.
[29] R. Diamant, "Closed form analysis of the normalized matched filter with a test case for detection of underwater acoustic signals," *IEEE Access*, vol. 4, pp. 8225–8235, 2016.

GEUNHWAN KIM was born in Daegu, South Korea, in 1992. He received the B.S. and M.S. degrees in electronics engineering from Kyungpook National University, Daegu, in 2015 and 2017, respectively, where he is currently pursuing the Ph.D. degree in electronics engineering. His research interests include array signal processing, underwater acoustic signal processing, and continuous active sonar.

KYUNKYUNG LEE (Member, IEEE) was born in Seoul, South Korea, in 1955. He received the B.S. degree in electronics engineering from Sogang University, Seoul, in 1977, and the M.S. and Ph.D. degrees in electronics engineering from The University of Texas at Austin, USA, in 1984 and 1987, respectively. From 1977 to 1982, he was a Researcher with the Agency for Defense Development, and from 1987 to 1989, he was an Assistant Professor with Oklahoma State University, Stillwater, OK, USA. Since 1989, he has been a Professor with the School of Electronics Engineering, Kyungpook National University, Daegu, South Korea. His research interests include array signal processing, underwater acoustic signal processing, and underwater distributed sensor networks.

SEOKJIN LEE (Member, IEEE) received the B.S., M.S., and Ph.D. degrees in electrical and computer engineering from Seoul National University, in 2006, 2008, and 2012, respectively.

From 2012 to 2014, he was a Senior Research Engineer with LG Electronics Inc., and from 2014 to 2018, he was an Assistant Professor with the Department of Electronics Engineering, Kyonggi University, Suwon, South Korea. Since 2018, he has been an Assistant Professor with the School of Electronics Engineering, Kyungpook National University, Daegu, South Korea. His research interests include acoustic, sound, and music signal processing, array signal processing, and blind source separation.